Reprinted from **Long-Range Correlations in Astrophysical Systems**
Volume 848 of the *Annals of the New York Academy of Sciences*
May 15, 1998

Two-Dimensional Vortex Crystals[a]

D. Z. JIN AND D. H. E. DUBIN

Physics Department, University of California at San Diego, La Jolla, California 92093

ABSTRACT: Magnetically confined pure electron columns evolve as nearly inviscid, incompressible two-dimensional (2-D) fluids. Experiments on these columns have found that the decay of 2-D turbulence leads to spontaneous formation of "vortex crystals," which are symmetric arrays of strong vortices within a background of lower vorticity. These vortex crystals can be described as maximum fluid entropy states for a system with an ergodically mixed background and a conserved number of strong vortices.

1. INTRODUCTION

The study of turbulence in inviscid, incompressible 2-D fluids is important for understanding geophysical and astrophysical flows [1], [2]. The Great Red Spot of Jupiter, for example, has been modeled in terms of inviscid 2-D Euler flow [3]. Magnetically confined pure electron columns are excellent systems for quantitative study of the free relaxation of 2-D turbulence. In a recent experiment on such columns, the vorticity $\omega(\mathbf{r}, t) = \nabla \times \mathbf{v}(\mathbf{r}, t)$ of the turbulent flow relaxed from some initial conditions to a "vortex crystal" equilibrium, which consists of small intense patches of vorticity (strong vortices) forming a stable equilibrium pattern in a low vorticity background [5]. These vortex crystal states have not been previously observed or predicted to form from turbulent initial conditions. Recently, we have shown that the vortex crystals can be described as the maximum fluid entropy states of a system with an ergodically mixed background and a conserved number of strong vortices [6]. In this paper we discuss the experiment and our theory for the vortex crystals.

2. THE EXPERIMENT

The experimental device is shown in FIG. 1. The electron columns are confined radially by a uniform magnetic field, B_z, and contained axially by voltage applied to end sections of the cylindrical walls. The z-averaged electron density $n(r, \theta, t)$ is accurately measured by dumping the column onto a phosphor screen imaged by a 512 $\times$ 512 CCD camera. Time evolution is inferred from a sequence of shots with differing hold times. This is possible because the shot-to-shot variations in the initial profiles can be controlled within small error.

[a]This work was supported by NSF grant PHY94-21318.

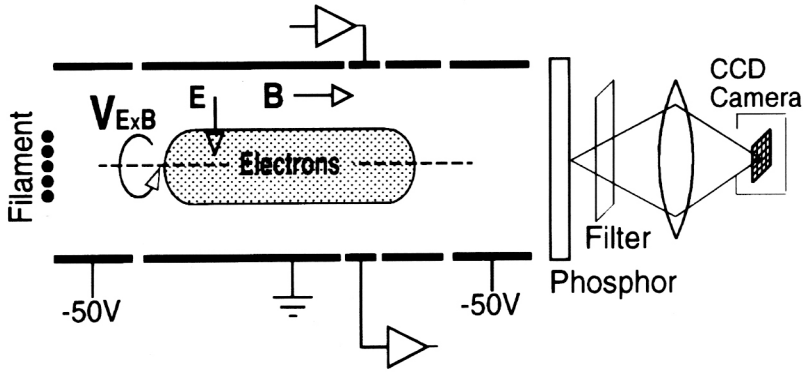

FIGURE 1. The cylindrical experimental apparatus with phosphor screen/CCD camera diagnostic.

In the experiment, the axial bounce frequency of an electron is large compared to the E × B drift rotation frequency; therefore, the evolution of $n(r, \theta, t)$ is described by the 2-D drift-Poisson equation, i.e.,

$$\frac{\partial n}{\partial t} + \mathbf{v} \cdot \nabla n = 0, \quad \mathbf{v} = -\frac{c}{B_z} \nabla \Phi \times \hat{\mathbf{z}}, \quad \nabla^2 \Phi = 4\pi e n. \tag{1}$$

These equations are isomorphic to the Euler equations for an incompressible inviscid 2-D fluid. The measured electron density is proportional to the vorticity of the flow, i.e., $\omega = 4\pi e c n/B_z$, and the electrostatic potential is proportional to the stream function ψ, i.e., $\psi = -c\Phi/B_z$. The nonzero $\partial\Phi/\partial r$ at the wall gives a true free-slip boundary condition.

Vortex crystals form from a highly filamented electron density distribution, as shown in FIG. 2(a). Within one turnover time of the electron column ($\tau_R = 170\ \mu s$), $N_v = 50$–100 strong vortices of roughly equal circulation form due to Kelvin-Helmholtz instabilities, as shown in FIG. 2(b). Subsequently, the turbulent state evolves and relaxes by chaotic vortex advection and mergers, as shown in FIG. 2(c). As a consequence, the number of the strong vortices decreases as $N_v \sim t^{-\xi}$, with $\xi \approx 1^5$. This relaxation is generally consistent with a dynamical scaling theory based on conserved quantities in repeated vortex merger [7].

However, the chaotic vortex motions eventually "cool" down and the vortices no longer merge. The strong vortices then relax into a lattice pattern, which rotates with the background, as shown in FIGS. 2(d) and 2(e). Seemingly, the increase of the number of strong vortices at $600\tau_R$ (FIG. 2(e)) compared to that at $60\tau_R$ (FIG. 2(d)) is because the initial conditions that lead to each image are slightly different owing to the shot noise. The vortex crystal states survive for about $10^4\tau_R$. After this period, individual vortices decay away and the remaining strong vortices adjust to a new rigidly rotating symmetric pattern.

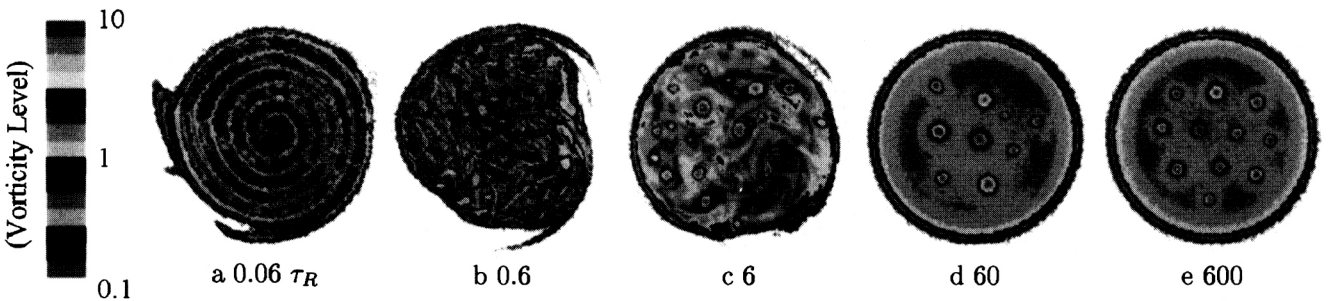

FIGURE 2. Formation of vortex crystal. False color contour plots of vorticity (represented in gray scale here) at five times are displayed. The unit of the vorticity is $\Gamma/r_\omega{}^2$, where r_ω is the radius of the conducting boundary.

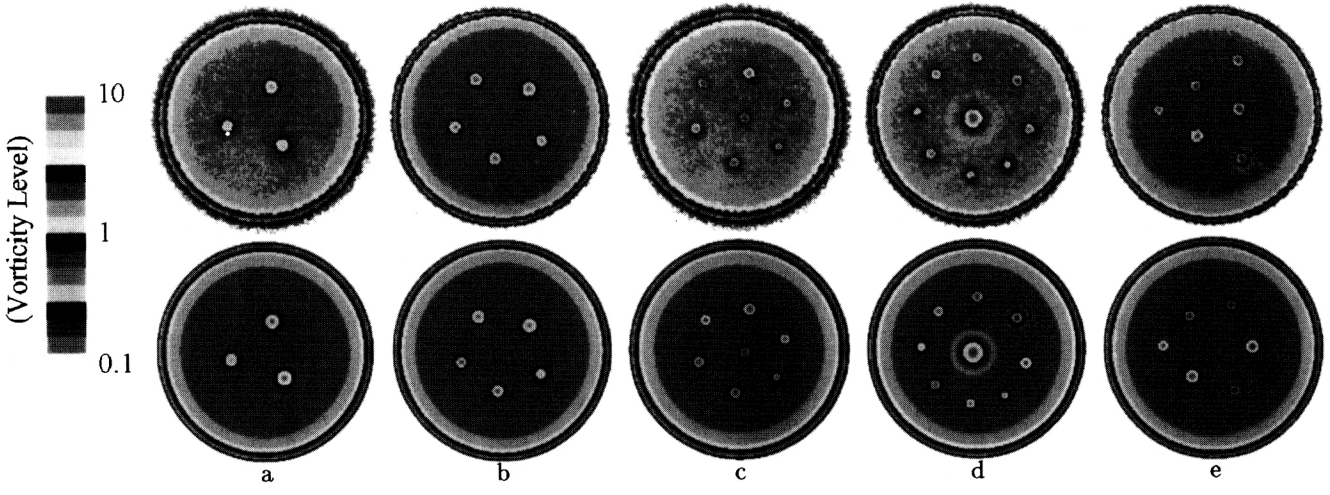

FIGURE 3. Top: examples of experimental images of vortex crystal states. Bottom: corresponding maximum fluid entropy states.

Experimentally, the evolution conserves total circulation Γ, angular momentum L, and energy H. Here

$$\Gamma = \int d\mathbf{r}^2 \omega, \tag{2}$$

$$L = -\int d\mathbf{r}^2 \omega r^2/2, \tag{3}$$

$$H = \int d\mathbf{r}^2 |\mathbf{v}|^2/2 = \int d\mathbf{r}^2 \psi\omega/2. \tag{4}$$

3. MAXIMUM FLUID ENTROPY THEORY

After the chaotic vortex mergers stop, the flow continues to evolve. The random motions of the strong vortices slowly "cool" as the vortices relax toward an equilibrium, and during this evolution the background also evolves. We have found that the final equilibrium of flow, the vortex crystal, can be described as a maximum fluid entropy state of a system with a low vorticity background and a conserved number of strong vortices. Two properties of the final states of the system can be predicted by the maximum fluid entropy theory: the distribution of the background vorticity $\omega_b(\mathbf{r})$, and the positions of the strong vortices $\mathbf{R}_i$, $i = 1, M$. Comparison between the theoretical predictions and the experimental data shows good agreement.

Maximization of the entropy of the system is constrained by the conservation of the total circulation, angular momentum and energy. These constraints follow from the dissipationless nature of ideal fluid flow, together with the cylindrical symmetry and free-slip boundary conditions of the experimental geometry. Also, the incompressibility of vorticity implies that infinitesimal vorticity elements can not overlap during their mixing, which provides another constraint.

The entropy associated with a macroscopic coarse-grained background vorticity distribution $\omega_b(\mathbf{r})$ can be calculated by counting the number of ways of arranging microscopic vorticity elements to obtain the given coarse-grained vorticity. For the simplest case of the microscopic vorticity elements having the same positive vorticity ω_f, the entropy is [8]:

$$S[\omega_b(\mathbf{r})] = -\int d\mathbf{r}^2 \left[\frac{\omega_b(\mathbf{r})}{\omega_f} \ln \frac{\omega_b(\mathbf{r})}{\omega_f} + \left(1 - \frac{\omega_b(\mathbf{r})}{\omega_f}\right) \ln\left(1 - \frac{\omega_b(\mathbf{r})}{\omega_f}\right) \right]. \tag{5}$$

The second term is due to the incompressibility of the vorticity elements, and does not appear in the usual (Boltzmann) expression of the entropy for a compressible flow. The contribution to the entropy from the positions of the strong vortices is negligible because the background has an infinite number of degrees of freedom. Therefore S is also the entropy of the entire (strong vortices + background) system.

The vorticity distribution of the strong vortices are assumed to be described by fixed axially symmetric functions $\omega_{v,i}(|\mathbf{r} - \mathbf{R}_i|)$. Since the vortices are quite intense and small, it does not make a great deal of difference what functional form one chooses for $\omega_{v,i}$ but we choose the (approximately Gaussian) form associated with

observed vortices. The stream function ψ is related to the vorticity ω of the flow via Poisson's equation

$$\nabla^2\psi = -\omega. \tag{6}$$

The maximization of S while keeping H, L, and Γ constant is done by the standard technique of Lagrange multipliers: $\delta F = 0$, where $F \equiv S - \beta(H - \Omega L + \mu\Gamma)$, and β, Ω, and μ are Lagrange multipliers that can be interpreted as inverse temperature, rotation frequency, and the chemical potential, respectively. Variation of F with respect to vortex positions $\{\mathbf{R}_i\}$ yields

$$\frac{\partial}{\partial \mathbf{R}_j}(H - \Omega L) = 0. \tag{7}$$

Since $H - \Omega L$ is the Hamiltonian of the system in the rotating frame of frequency Ω, the above equation shows that in the maximum entropy state, the velocity of the strong vortices is zero in this rotating frame: in other words, the strong vortices are in equilibrium, rotating rigidly at frequency Ω. Furthermore, since S is maximized, this equilibrium must be stable.

Variation of F with respect to the background vorticity $\omega_b(\mathbf{r})$ yields the coarse-grained background vorticity:

$$\omega_b(\mathbf{r}) = \frac{\omega_f}{e^{\beta\omega_f\phi} + 1}, \tag{8}$$

where $\phi \equiv \psi + \frac{1}{2}\Omega r^2 + \mu$ is the stream function in the rotating frame. This is very similar to the Fermi distribution in quantum statistics. Equations (7) and (8) characterize the maximum fluid entropy states of our system.

In order to test whether experimentally observed vortex crystal states can be explained by the maximum fluid entropy states, the predictions of the theory are compared with the experimental data. The maximum fluid entropy states are calculated by numerically solving Eqs. (6) and (7). Since the vorticity in the background is given by Eq. (8), Eq. (6) is a 2-D nonlinear partial differential equation. Parameters β, Ω, μ, and $\{\mathbf{R}_i\}$ are searched to obtain the maximum fluid entropy state for given conserved quantities H, L, Γ, as well as the M vorticity distributions $\omega_{v,i}$ of the strong vortices. In general, there may be several possible patterns of the strong vortices, representing local maxima of the entropy. To obtain maximum entropy states close to the experimental vortex crystals, we use the experimental positions of the strong vortices as the initial values of the search. The procedure we employed to determine M and $\omega_{v,i}$ from the experimental data is essentially that of McWilliams [9].

The complete specification of the problem requires the choice of a value for the Fermi vorticity ω_f associated with the microscopic background vorticity elements. Although in general ω_f can have a distribution of vorticity levels [8], a single value is found to be sufficient to explain the experiments. The maximum of the measured vorticity is taken as ω_f. This choice is based on the following considerations: ω_f must be larger than or equal to the maximum observed background vorticity level, which is coarse-grained by the experimental imaging system; since the observed vortex

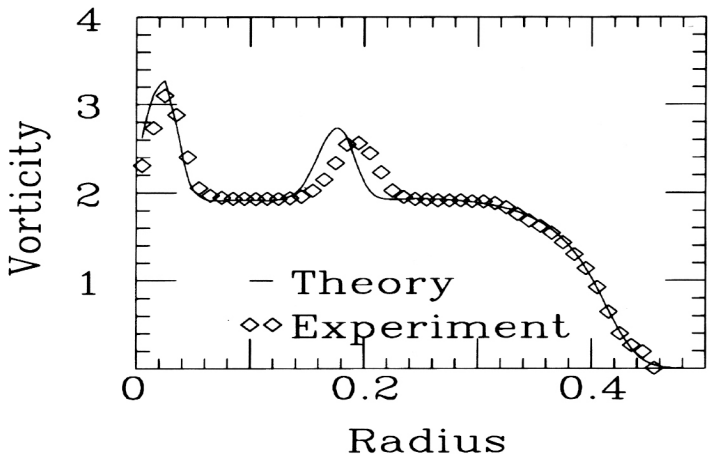

FIGURE 4. The θ-averaged vorticity profile from the five vortex state of FIG. 3(c).

crystal states appear to be nearly Fermi-degenerate, in some finite region of the background the coarse-grained vorticity should approach ω_f. The following fundamental units are used to renormalize the physical quantities: length is r_w (radius of the circular conducting boundary) and vorticity is Γ/r_w^2.

The theory agrees well with the experimental data. The calculation reproduces the observed vortex crystal patterns, as shown in FIG. 3, in which selected experimental images of vortex crystals and their corresponding maximum fluid entropy states are displayed. Although there is a slight azimuthal asymmetry and some noise in some experimental images, the observed background vorticity is close to the theory, as shown in the θ-averaged vorticity profiles in FIG. 4. The background of the finite temperature solutions has the following features: The edge falls off over a scale related to the fluctuation energy $1/\beta$ of the vorticity elements near the edge, as in FIG. 4; and near a strong vortex the background vorticity is slightly depressed, since ϕ tends to increase due to the influence of the strong vortex, as observed around the large central vortex in FIG. 3(d).

4. DISCUSSION

The maximum fluid entropy theory is successful in describing the vortex crystal states. This provides us with an intuitive picture of vortex crystal formation after strong vortices have formed: the turbulent evolution ergodically mixes certain regions of the flow (the background) and this process causes the unmixed regions of strong vorticity to relax to an observed equilibrium pattern (the crystal). The increase in the order of the strong vortices during this process is offset by the increased disorder in the background, as expected from the second law of thermodynamics.

However, maximum fluid entropy theory does not answer many interesting questions related to the dynamics of vortex crystal formation. For example, the details of the mixing process and the rate at which strong vortices relax to the equilibrium patterns remain to be investigated. Also, experimentally, vortex crystals are not formed from some initial conditions that are similar to those that do lead to the formation of vortex crystals [5]. The characteristics of the initial conditions for vortex crystals is still unknown.

REFERENCES

1. McWilliams, J.C. 1983. On the relevance of two-dimensional turbulence to geophysical fluid motions. J. Méc. Theor. Appl., Spec. Suppl. 83–97.
2. Ingersoll, A.P. 1990. Atmospheric dynamics of the outer planets. Science. **248:** 308–315.
3. Marcus, P.S. 1988. Numerical simulation of Jupiter's Great Red Spot. Nature **331:** 693–696.
4. Driscoll, C.F. & K.S. Fine. 1990. Experiments on vortex dynamics in pure electron plasmas. Phys. Fluids. **2:** 1359–1366.
5. Fine, K.S., A.C. Cass, W.G. Flynn & C.F. Driscoll. 1995. Relaxation of 2D turbulence to vortex crystals. Phys. Rev. Lett. **75:** 3277.
6. Jin, D.Z. & D.H.E. Dubin. Phys. Rev. Lett. Accepted for publication.
7. Carnevale, G.F. *et al.* 1991. Evolution of vortex statistics in two-dimensional turbulence. Phys. Rev. Lett. **66:** 2735–2737.
8. Miller, J. 1990. Statistical mechanics of Euler equations in two dimensions. Phys. Rev. Lett. **65:** 2137–2140; Robert, R. & J. Sommeria. 1991. Statistical equilibrium states for two-dimensional flows. J. Fluid Mech. **229:** 291–310.
9. McWilliams, J.C. 1990. The vortices of two-dimensional turbulence. J. Fluid Mech. **219:** 361–385.